Progress In Electromagnetics Research B, Vol. 25, 53–74, 2010

MINIATURE AND HIGHER-ORDER MODE FERRITE MIMO RING PATCH ANTENNA FOR MOBILE COMMUNICATION SYSTEM

S. Bae, Y.-K. Hong, J.-J. Lee, J.-H. Park, J. Jalli, and G. Abo

Department of Electrical and Computer Engineering
and MINT Center
The University of Alabama
Tuscaloosa, AL 35487, USA

H.-M. Kwon and C. K. K. Jayasooriya

Department of Electrical Engineering and Computer Science
Wichita State University
Wichita, KS 67260, USA

Abstract—Miniaturized ferrite ring patch antennas (RPAs) were designed and fabricated for multiple-input multiple-out (MIMO) applications. Design parameters of higher-order mode ferrite RPAs, 1-RPA and 2-RPA, were optimized, and antenna performance of the ferrite 1-RPA was evaluated. The Z-type hexaferrite and 2%-weight borosilicate glass composite was used for the ferrite antenna disk. The measured permeability (μ_r) and permittivity (ε_r) of the hexaferrite were 2.59 and 5.7, respectively, at 2.5 GHz. Three-mode orthogonal radiation of the ferrite 1-RPA was experimentally confirmed. With regard to the ferrite 2-RPA, excellent isolation (−40 dB) between ports 1 and 2 was achieved at 2.5 GHz. This excellent isolation property is attributed to both mode 3 orthogonal radiations of the bottom and top RPAs. The volumes of the 1- and 2-RPA were reduced to 14.5% and 34.5%, respectively, from 95 cm^3 of a dielectric 2-circular patch antenna (2-CPA) volume.

1. INTRODUCTION

Recently, a high data transmission rate is needed for mobile wireless local area networks (W-LANs), WiMax, and long-term evolution

Received 19 July 2010, Accepted 17 August 2010, Scheduled 20 August 2010
Corresponding author: Y.-K. Hong (ykhong@eng.ua.edu).

(LTE) applications. The multiple-input multiple-output (MIMO) wireless communication system has been extensively researched [1, 2] due to its higher data transmission rate than the single-input single-output (SISO) system in a rich multipath environment. The data transmission rate is proportional to the number of antennas in the MIMO system. However, the MIMO system requires large antenna spacing, e.g., half λ (wavelength at carrier frequency), between adjacent antenna array elements to ensure that transmitted/received signals through different antenna elements are independent. It is also known that a closer distance than 10λ between antennas leads to poor electrical isolation properties. The electrical isolation between the antennas should be less than -20 dB to maintain the performance of the MIMO system. This is a challenging issue, because the size of mobile communication devices is limited.

It has been demonstrated that two orthogonal radiation patterns could be generated by the two dielectric circular patch antenna (2-CPA or dielectric 2-CPA) with mode number $n = 3$ for the MIMO applications [3–6]. Un-overlapped radiation patterns in the xy-plane with 30° displacement between radiation patterns can be achieved with both of the CPAs. Excellent isolation properties (much less than -20 dB) were achieved due to these un-overlapped radiation patterns. However, the large antenna size of the 2-CPA (diameter of CPA = 10.5 cm) is a current issue to address.

Ferrite has been previously reported to reduce the antenna length but, more importantly, the volume of the antenna [7–9]. This is because the ferrite possesses permeability (μ) and permittivity (ε), where μ and ε influence electromagnetic (EM) wave velocity υ and wavelength λ ($\upsilon = c/\sqrt{\mu\varepsilon},\ \lambda = \lambda_0/\sqrt{\mu\varepsilon}$). Therefore, Z-type hexaferrite was used to miniaturize antenna for mobile MIMO communication systems in this study. In this paper, a ferrite ring patch antenna (RPA) was proposed to further miniaturize the MIMO antenna. The effects of design parameters for the 1-RPA on antenna performance were investigated for 2.5 GHz MIMO system. Accordingly, the 1-RPA was fabricated using selected design parameters to evaluate its antenna performance. In addition, antenna performance of the ferrite 2-RPA was simulated and compared to the dielectric 2-CPA.

2. EXPERIMENTAL

2.1. Design Parameters

In order to generate mode 3 orthogonal radiation patterns of the small MIMO antenna, the ferrite 1- and 2-RPA structures are proposed, as shown in Figs. 1(a), (b), and (c). Ring width, ferrite disk

thickness, permeability and permittivity of ferrite, its loss tan δ, and permeability/permittivity ratio were chosen for the design parameters of the ferrite RPA. In order to optimize design parameters, antenna performance was simulated by Ansoft HFSS software based on 3D finite element method (FEM) simulation. The selected design parameters of the bottom RPA were 31.9 mm and 6.5 mm of radius and thickness, respectively, while those of the top RPA were 25 mm and 7 mm of radius and thickness, respectively. In addition, permeability and permittivity of the bottom and top ferrite disks were found to be 2.2, 4.5 and 2.3, 7.0, respectively, at 2.5 GHz.

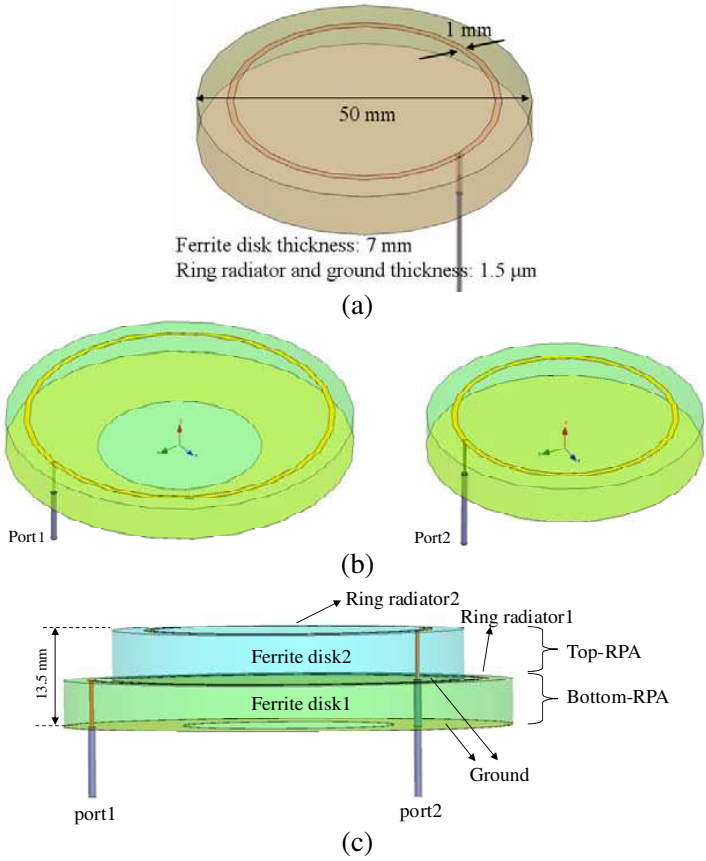

Figure 1. Structure of (a) 1-RPA, (b) bottom- and top-RPA for 2-RPA and (c) side view of 2-RPA.

2.2. Fabrication

Several spinel ferrites and hexaferrites are used for MHz ∼ GHz device applications with the permeabilities and permittivities given in Table 1. Among the hexaferrites, soft Z-type hexaferrite ($Ba_3Co_2Fe_{24}O_{41}$) shows the highest permeability. Therefore, Z-type hexaferrite was used in this study for the substrate material of ferrite RPA.

The one-step mixing and calcination process (MCP) [23] was used to synthesize the Z-type hexaferrite particles for fabrication of the ferrite ring and disk. The water-quenching process was included in the MCP to obtain high purity hexaferrite fine particles. This detailed process has been reported in [22, 23]. The ferrite ring (Inner diameter: 3 mm, outer diameter: 7 mm) and disk (25 mm of radius, 7 mm of thickness) were prepared by sintering in O_2 at 950°C for 1 h to obtain permeability and permittivity spectra. Permeability of sintered ferrite was adjusted by the addition of borosilicate glass to hexaferrite. On the other hand, Fig. 2 shows the flow chart for fabrication of the 1-RPA with the Z-type hexaferrite disk. After having prepared the Z-type hexaferrite disk, a hole was formed through the disk thickness. Then the hole was filled with conductive paste. The radiator and ground were prepared by sputter deposition of copper. Lastly, a coaxial cable was connected to the radiator and ground.

An x-ray diffractometer, vibrating sample magnetometer, network analyzer (Agilent N5230A), and coaxial air line fixture (Agilent 85051-60007) were used to characterize the static and dynamic magnetic

Table 1. Permeability and permittivity of ferrites.

		μ	ε	μ/ε
Spinel ferrite	Ni-Zn ferrite	95~100 at 5 MHz [10]	10 ~ 12 [11]	8.9
	Mn-Zn ferrite	5000 at 30 kHz [12]	450 at 100 kHz [13]	11.1
	Li-Zn ferrite	25 at 90 MHz [14]	200 ~ 500	< 0.125
	Li-Mn ferrite	-	600 at 4 MHz [15]	-
	YIG	5.2 at 400 MHz [16]	15.45 at 8 GHz [17]	0.337
	Ni-Zn-Cu ferrite	40~50 at 30 MHz [18]	20~25 at 4 MHz [19]	2.0
Hexagonal ferrite	M-type Ba ferrite	1.3 at GHz range [20]	11 at 1 GHz [21]	0.12
	Z-type Ba ferrite	8~10 at 300 MHz [22, 23]	8~10 at 300 MHz [22, 23]	1.0
	Y-type Ba ferrite	11 at 400 MHz [24]	15~18 at 1 GHz [25]	0.67
	Sr ferrite composite	3 at GHz range [26]	7.5 at GHz range [26]	0.4

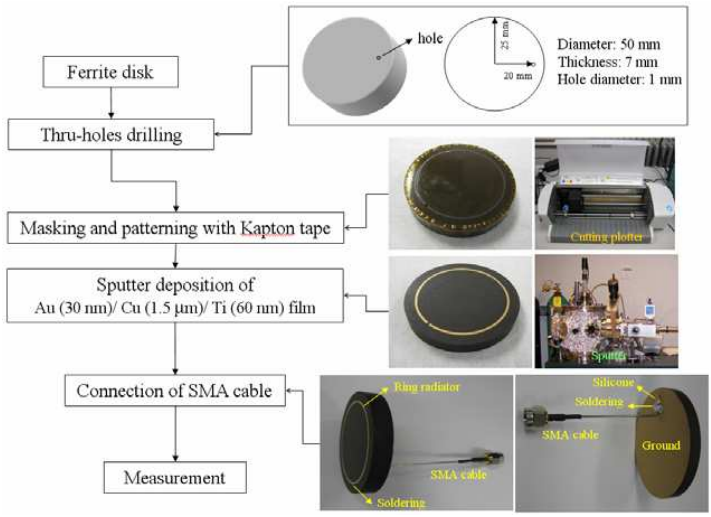

Figure 2. Flow chart for 1-RPA fabrication.

properties of the Z-type hexaferrites. An anechoic chamber system and network analyzer (Agilent ENA 5070B) were used to evaluate antenna performance.

3. RESULTS AND DISCUSSION

3.1. Design of RPA

The resonance mode number, n, of the CPA gradually increases with an increase in the radius of the circular radiator [3, 4]. From our simulated results, it was found that the relationship between n and the radius of the circular radiator is also valid in the RPA. Fig. 3 shows the simulated gain pattern of the 1-RPA at $n = 3$. All gain lobes are symmetrical about the center of the radiator, while the center of the radiator shows cavity resonance. The total number of gain lobes is two times n.

With regard to the 2-RPA, two individual mode-3 gain patterns from ports 1 and 2 can be obtained with a $30° + 60°N$ (where N is an integer) angle between ports 1 and 2 from the center of the radiator as shown in Fig. 1(c). Thus, the six gain lobes of port 2 are taking the six null directions of the six gain lobes of port 1, which means interference between ports 1 and 2 can be minimized by the separated orthogonal radiations of the 2-RPA. Therefore, electromagnetic signals from ports 1 and 2 of the 2-RPA are completely isolated for MIMO antenna applications.

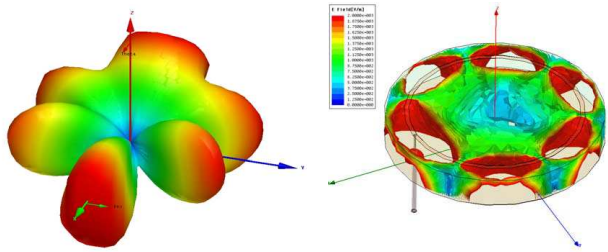

(a) (b)

Figure 3. (a) 3D gain pattern and (b) inner-electric field distribution for ferrite 1-RPA.

Some equations describing electric field and antenna performance for the CPA or RPA are given by Equations (1) $\sim$ (8). Far-field components of the RPA for θ (elevation angle) and ϕ (azimuthal angle) are defined by Equations (1) and (2) [3–6, 27].

$$E_{a\theta}^{(n)} = e^{jn\pi/2}\frac{V_0^{(n)}}{2}(k_0 a)\cos n(\phi-\phi_0)(J_{n+1}-J_{n-1}) \quad (1)$$

$$E_{a\phi}^{(n)} = e^{jn\pi/2}\frac{V_0^{(n)}}{2}(k_0 a)\cos\theta\sin n(\phi-\phi_0)(J_{n+1}-J_{n-1}) \quad (2)$$

where a is the radius of the ring radiator, n is the resonance mode number, $V_0^{(n)}$ is the input voltage, k_0 is the free space propagation constant, ϕ_0 is the reference angle corresponding to the feed point of the antenna, and $J_N = J_N(k_0 a\sin\theta)$ is the Bessel function of the second kind (Neumann function, where N is an integer). The radius a at a given resonance mode can be calculated by Equation (3).

$$a = \frac{\chi_n'\lambda}{2\pi\sqrt{\mu_r\varepsilon_r}} \quad (3)$$

where χ_n' is the first zero of the derivative of the Bessel function J_n, λ is the wavelength at a given frequency, μ_r is the relative permeability, and ε_r is the relative permittivity. The values of χ_n' are 1.8412, 3.0542, 3.8318, and 4.2012, with resonance modes $n = 0$, 1, 2, and 3, respectively. Therefore, a at $n = 3$ can be calculated by Equation (4).

$$a = \frac{4.2012\lambda}{2\pi\sqrt{\mu_r\varepsilon_r}} = \frac{4.2012c}{2\pi f\sqrt{\mu_r\varepsilon_r}} \quad \text{for } n = 3 \quad (4)$$

where c is the light velocity and f is the resonant frequency.

Figure 4 presents the calculated resonant frequency as a function of radius a by Equation (4). It can be seen that the resonance frequency

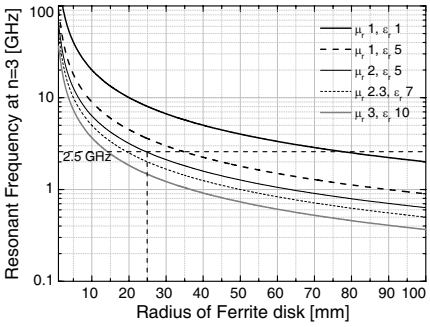

Figure 4. Resonant frequency of ferrite 1-CPA as a function of disk radius.

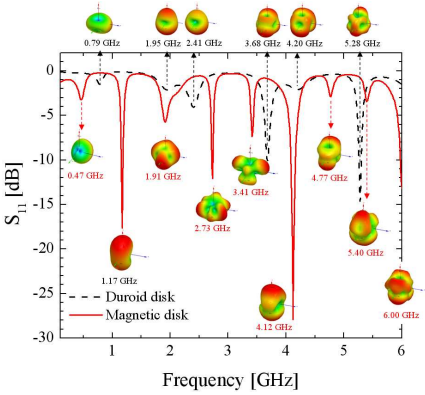

Figure 5. Frequency dependence of S_{11} parameters for dielectric Duroid and magnetic ferrite disk antennas.

exponentially decreases with the radius of the CPA (or RPA), and the mode-3 resonant frequency of 2.5 GHz can be obtained with 2 of μ_r and 5 of ε_r for a ferrite disk having a radius of 25 mm.

The simulated S-parameter and 3D gain pattern of the 25 mm radius Duroid ($\mu = 1$, $\varepsilon = 2.2$) RPA and ferrite ($\mu = 2.3$, $\varepsilon = 6$) RPA with a 21 mm radius ring are presented in Fig. 5. Mode 3 resonant frequency of the ferrite RPA is obtained to be 2.73 GHz, while that for the Duroid RPA is estimated to be 5.28 GHz. This suggests that the radius of the Duroid RPA can be reduced by the ferrite RPA.

With regard to magnetic loss, it has been reported that a tangent of 0.03 of magnetic loss is acceptable to achieve 55% radiation efficiency [28]. Meanwhile, bandwidth of the CPA or RPA is greatly decreased with ε_r rather than μ_r, as suggested by Equation (5) [29].

$$BW = \frac{96\sqrt{\mu_r/\varepsilon_r}}{\sqrt{2}\left(4 + 17\sqrt{\mu_r\varepsilon_r}\right)}\frac{t}{\lambda_0} \quad (t = \text{thickness of disk}). \tag{5}$$

For the antenna size limit, Chu's equations, Equations (6) and (7) [30–33], are used to estimate theoretical bandwidth and radiation efficiency for the proposed 2-RPA.

$$Q = \frac{1}{(ka)^3} + \frac{1}{ka}, \tag{6}$$

where k, a, and V are

$$k = \frac{2\pi}{\lambda}, \quad a = \left(\frac{3V}{4\pi}\right)^{\frac{1}{3}}, \quad V = \frac{4}{3}\pi a^3$$

Therefore, Equation (6) becomes

$$FBW^{-1} = Q = \frac{1}{(ka)^3} + \frac{1}{ka} = \frac{1}{6\pi^2 Vol} + \frac{1}{2\pi(\frac{3}{4\pi})^{\frac{1}{3}} Vol^{\frac{1}{3}}}, \quad (7)$$

where normalized volume (Vol) is

$$Vol = \frac{V}{\lambda^3}$$

The results are presented in Fig. 6. The quality factor with radiation loss is defined by Equation (8).

$$Q_{Lossy} = \eta Q_{Lossless} \quad (8)$$

where η is the radiation efficiency of the antenna.

A wavelength of 120 mm and Q-factor of 10 are estimated under the assumption of the center frequency (f_c) of 2.5 GHz, bandwidth (BW) of 250 MHz, fractional bandwidth (FBW) of 10%, and radiation efficiency (η) of 100%. Therefore, the normalized volume (V/λ^3) is about 0.002, which results in the antenna V (volume) of 3,500 mm^3. This is the Chu's volume limit. The volume of the proposed top RPA, which is smaller than the bottom RPA, is 13,738 mm^3 (disk radius = 25 mm, thickness = 7 mm), the volume of which is about four times larger than the Chu's volume limit. Therefore, the 1-RPA size is far from the Chu's volume limit at 2.5 GHz and 100% radiation efficiency. This implies that further optimization or miniaturization is possible.

In order to optimize design parameters for the 2.5 GHz RPA, antenna performance with various design parameters was evaluated and optimized by a simulation technique. The radius of the disk and ring radiator, thickness of the disk, permeability, and permittivity were

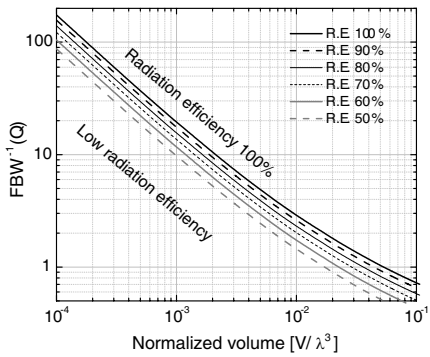

Figure 6. Volume dependence of Q with various radiation efficiencies.

fixed to be 31.9 mm, 28 mm, 6.5 mm, 2, and 5, respectively, for the simulation. Fig. 7 shows the frequency dependence of S_{11}-parameters and gain patterns of RPA for ring width ranging from 1 to 6 mm. The center frequency (f_c) is slightly moved to 2.39 GHz from 2.475 GHz as the ring width increases. This change of f_c is attributed to the increased capacitive coupling between the ring radiator and ground due to the increased area of the ring. On the other hand, there is almost no change in gain pattern with an increase in ring width.

The frequency dependence of the S_{11}-parameter and gain patterns of the RPA with various disk thicknesses, and distance between ground and radiator are presented in Fig. 8 when radius of ring is 28 mm. Here the gain is significantly increased by the increase in disk thickness, but

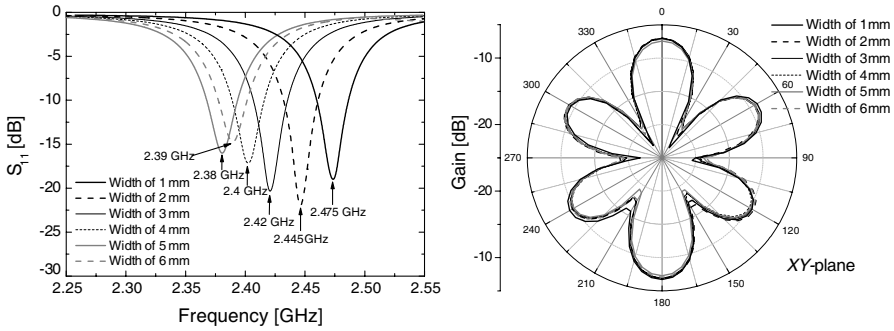

Figure 7. (a) Frequency dependency of S_{11} and (b) gain patterns for 1-RPA with various widths of ring.

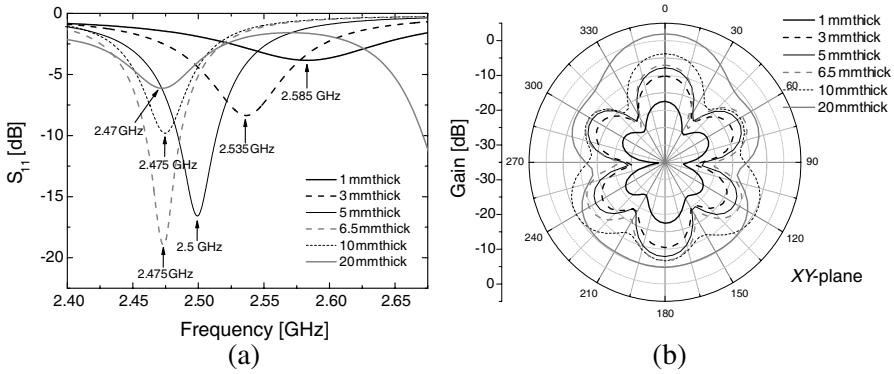

Figure 8. (a) Frequency dependency of S_{11} and (b) gain patterns for 1-RPA with various thicknesses of disk.

f_c is slightly decreased. The orthogonal pattern is clarified as disk thickness increases from 1 to 6.5 mm, as shown in Fig. 8(b). The orthogonal pattern gradually disappears with increasing the thickness greater than 6.5 mm. This is attributed to the capacitive ground coupling. A strong capacitive coupling occurs with thinner disk and a narrow gap between the ground and the radiator, and leads to weak electromagnetic radiation. On the other hand, high disk thickness leads to weak capacitive coupling. In this case, the mode 3 orthogonal radiation property of the RPA disappears due to the weak ground coupling.

The effect of antenna substrate properties, μ_r and ε_r, on the antenna performance was also studied. The simulated results show that μ_r improves the antenna performance of the RPA. The f_c is dramatically decreased as μ_r is increased from 1 to 5, with ε_r fixed at 1, as shown in Fig. 9(a). In addition, the maximum gain is increased and the orthogonal gain pattern is obviously clarified by the increase in μ_r.

On the other hand, the increase in ε_r is effective in the lowering of f_c and clarifying of the orthogonal gain pattern and the maximum gain is decreased. Fig. 10(a) shows that f_c rapidly decreases from 5.4 GHz to 3.12 GHz with an increase in ε_r. The orthogonal gain pattern for ε_r from 2 to 5 is shown in Fig. 10(b). These are due to the increased capacitance by ε_r. Accordingly, the f_c is lowered, but gain is decreased. Therefore, it is concluded that μ_r, rather than ε_r, is the effective design parameter for antenna performance.

Considering the realizable ferrite property, the ε_r was fixed at

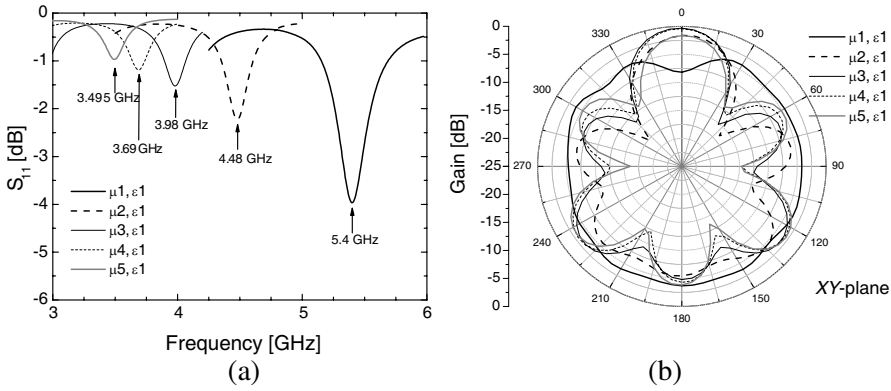

Figure 9. (a) Frequency dependency of S_{11} and (b) gain patterns for 1-RPA with various permeabilities of disk.

5, and the performance of the RPA with μ_r ranging from 1 to 5 was evaluated. It was found that the f_c rapidly decreased from 3.12 to 1.885 GHz with an increase in the ratio of μ_r/ε_r from 1 to 5 as shown in Fig. 11(a). Maximum gain also decreased from -3.46 to -13.64 dB with 1/5 to 5/5 ratio of μ_r/ε_r, as shown in Fig. 11(b), which is attributed to the decreased antenna size from 0.291λ at 3.12 GHz to 0.176λ at 1.885 GHz. Consequently, antenna volume is close to the Chu's limit volume, and therefore, resulting in radiation efficiency.

Furthermore, the effects of magnetic and dielectric loss on the performance of the RPA were evaluated. Figs. 12 and 13 show

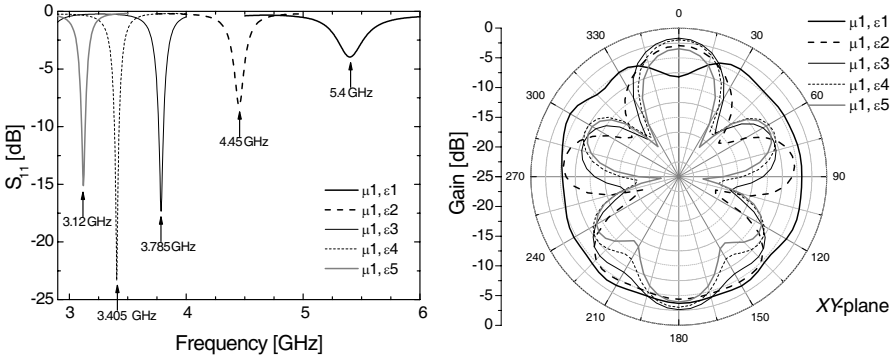

Figure 10. (a) Frequency dependency of S_{11} and (b) gain patterns for 1-RPA with various permittivities of disk.

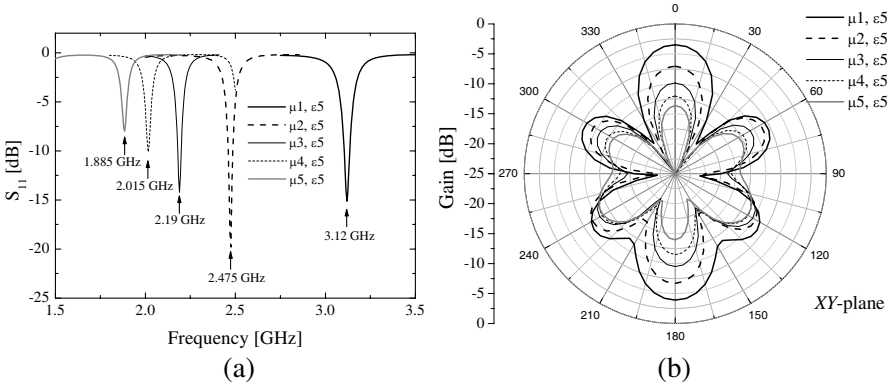

Figure 11. (a) Frequency dependency of S_{11} and (b) gain patterns for 1-RPA with various permeabilities/permittivity of disk.

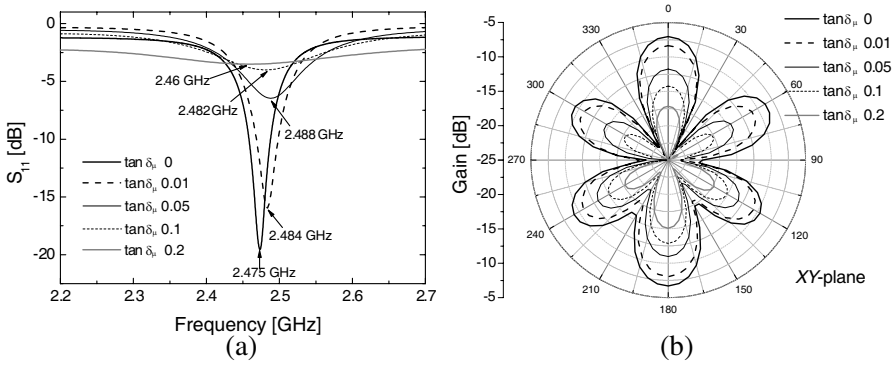

Figure 12. (a) Frequency dependency of S_{11} and (b) gain patterns for 1-RPA with various loss $\tan\delta_\mu$ of disk.

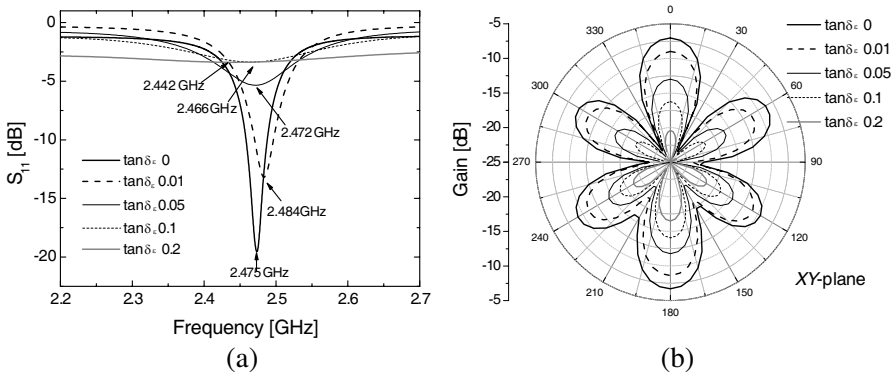

Figure 13. (a) Frequency dependency of S_{11} and (b) gain patterns for 1-RPA with various loss $\tan\delta_\varepsilon$ of disk.

the effects of magnetic and dielectric loss $\tan\delta$, respectively. Both figures show the same results of mismatched S_{11}-parameter, broadened bandwidth and decreased maximum gain with the increase in both loss $\tan\delta$. These results are attributed to the increased energy dissipation with the increase in both loss factors, $\tan\delta$; therefore, the quality factor of radiation is decreased and then bandwidth is increased.

The effect of the aforementioned design parameters on the performance of RPA is summarized in Table 2.

Table 2. Effect of design parameters on antenna performance.

	$f_{\#3}$	$\text{Gain}_{\max}$	Δ Gain	BW	Selected
Width	•				1 mm
Thickness	•	○○○	○(up to 6.5)		6.5 mm
μ	••	○	○	•	~ 2
Tan δμ		•••	•	○○○	< 0.01
ε	•••	•	○	•	~ 5
Tan δε		•••	•	○○○	< 0.01

Δ Gain: $\text{Gain}_{\max} - \text{Gain}_{\min}$ on xy-plane
○○○: very proportional
○○: proportional
○: little proportional
•••: very inversely proportional
••: Inversely proportional
•: little inversely proportional

3.2. Ferrite for RPA

The theoretical maximum μ_r of ferrite at 2.5 GHz was calculated to estimate the achievable μ_r. The intrinsic complex μ_r of ferrite can be calculated using the Landau-Lifshitz-Gilbert (LLG) Equations (9), (10), and (11).

$$\begin{aligned}\mu_r(\omega) &= \mu_r(\omega)' - j\mu_r(\omega)'' \\ &= 1 + \frac{\gamma 4\pi M_S}{\gamma H_k + j\alpha\omega} \times \left[1 + \frac{\omega^2}{(\gamma H_k + \gamma 4\pi M_s + j\alpha\omega)(\gamma H_k + j\alpha\omega) - \omega^2}\right] \quad (9)\end{aligned}$$

$$\mu_r' = \frac{4\pi M_s}{H_k} \cdot \frac{\omega_r^2\left(\omega_r^2 - \omega^2\right)}{\left(\omega_r^2 - \omega^2\right)^2 + \left(4\pi_\alpha \gamma M_s \omega\right)^2} \quad (10)$$

$$\mu_r'' = \frac{4\pi M_s}{H_k} \cdot \frac{\omega_r^2\left(4\pi\alpha\gamma M_s\omega\right)}{\left(\omega_r^2 - \omega^2\right)^2 + \left(4\pi\alpha\gamma M_s\omega\right)^2} \quad (11)$$

where ω represents the angular driving frequency ($\omega = 2\pi f$), α is the damping constant and γ represents the gyromagnetic ratio (1.76×10^7 rad/Oe sec). The calculated effective complex permeability spectra of $\mu_r(\omega)'$ and $\mu_r(\omega)''$ were shown in Fig. 14. The 0.1 of α, 275 emu/cc of saturation magnetization (M_s), and 2100 Oe of magnetic anisotropy field (H_k) were used for the calculation. The theoretical maximum μ_r at 2.5 GHz is calculated to be 2.6, with 0.03 of magnetic loss $\tan\delta_\mu$.

Furthermore, the demagnetizing factor (N_d) needs to be considered for calculation of the effective permeability of the ferrite

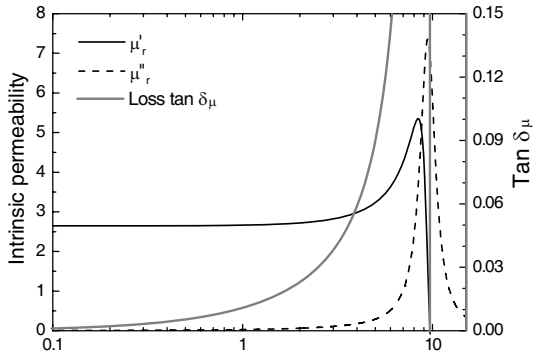

Figure 14. Calculated intrinsic permeability spectra by LLG equation.

disk. The N_d of the ferrite oblate (radius a $\neq$ radius b = radius c) can be calculated with Equations (12) and (13) [34].

$$N_{d,perp} = \frac{A_r^2}{A_r^2 - 1}\left(1 - \sqrt{\frac{1}{A_r^2 - 1}}\sin^{-1}\frac{\sqrt{A_r^2 - 1}}{A_r}\right) \tag{12}$$

$$N_{d,hori} = \frac{1 - N_{d,perp}}{2} \tag{13}$$

where the aspect ratio (A_r) is defined as

$$A_r = \frac{b}{a} = \frac{c}{a}$$

The calculated N_d as a function of aspect ratio for the ferrite oblate is presented in Fig. 15(a). Then the effective magnetic anisotropy field can be calculated by Equation (14).

$$H_{keff} = H_k + N_d M_s \tag{14}$$

Therefore, Equations (10) and (11) can be rewritten as Equations (15) and (16) to calculate effective complex permeability ($\mu_{r\text{-}eff}$).

$$\mu_{r\text{-}eff}{}' = \frac{4\pi M_s}{H_k + N_d M_s} \cdot \frac{\omega_r^2\left(\omega_r^2 - \omega^2\right)}{\left(\omega_r^2 - \omega^2\right)^2 + \left(4\pi\alpha\gamma M_s\omega\right)^2} \tag{15}$$

$$\mu_{r\text{-}eff}{}'' = \frac{4\pi M_s}{H_k + N_d M_s} \cdot \frac{\omega_r^2\left(4\pi\alpha\gamma M_s\omega\right)}{\left(\omega_r^2 - \omega^2\right)^2 + \left(4\pi\alpha\gamma M_s\omega\right)^2} \tag{16}$$

The A_r, $N_{d,perp}$, and $N_{d,hori}$ of the designed ferrite disks for the 2-RPA were 4.9 (= 3.19/0.65), 0.74, and 0.13, respectively, for the

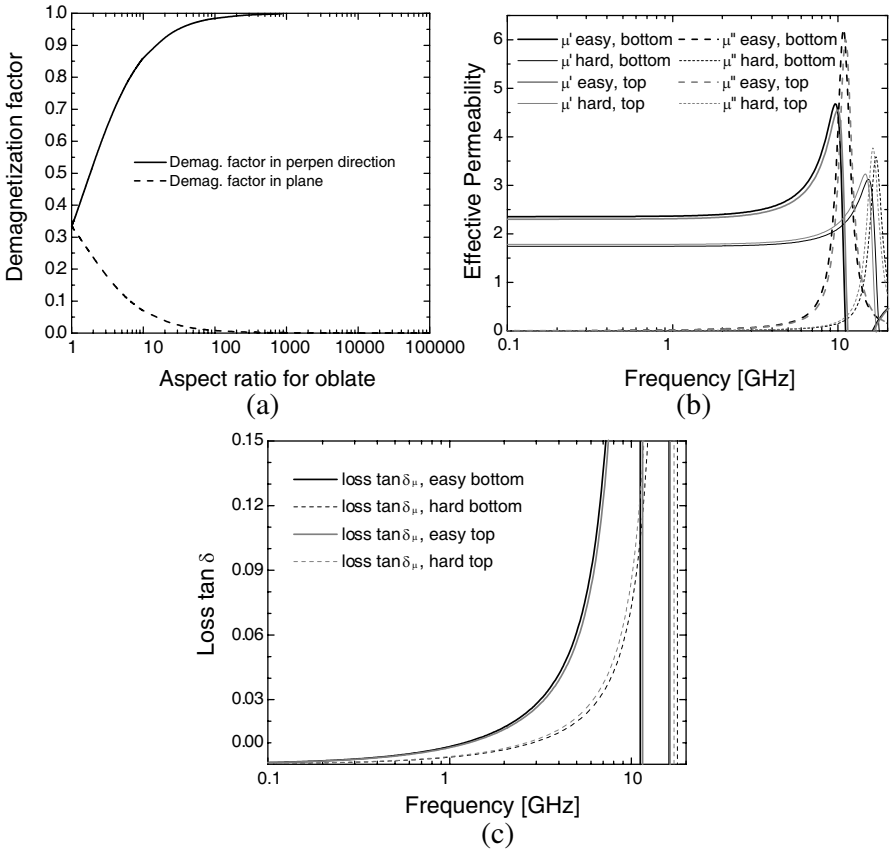

Figure 15. (a) Calculated demagnetizing factor as a function of aspect ratio of oblate, (b) effective permeability spectra and (c) loss tan δ_μ for ferrite 2-RPA.

bottom RPA and 3.6 (= 2.5/0.7), 0.67, and 0.16, respectively, for the top RPA. These values were used to calculate the μ_{r_eff} of the ferrite disks, as presented in Fig. 15(b). Also, the calculated $\tan\delta$ of the ferrite disks as a function of frequency is shown in Fig. 15(c).

In order to estimate the permeability of ferrite at f_c of 2.5 GHz, the Z-type hexaferrite ring and block as an antenna substrate were prepared by the sintering process. Glass, Bi_2O_3 and $CaCO_3$, were added to the Z-type hexaferrite to lower the sintering temperature. The melting temperatures of these agents are in the range of $820 \sim 830$°C. However, Bi_2O_3 and $CaCO_3$ are soluble in hydrochloric and sulfuric acid, which are commonly used for metal electroplating or wet-etching

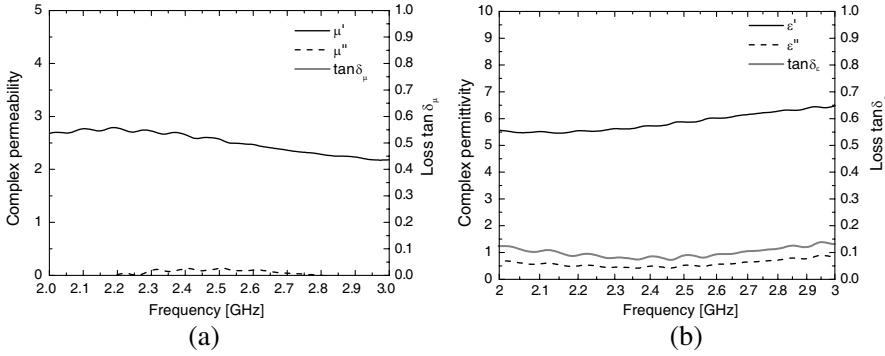

Figure 16. (a) Complex permeability and (b) permittivity of Z-type hexagonal ferrite.

processes. Borosilicate glass was chosen for the sintering agent to fabricate of hexaferrite-glass composite substrate.

A higher ferromagnetic resonance (FMR) frequency than 3 GHz and relatively low ε_r can be achievable with the hexaferrite-glass composite, similar to hexaferrite particles embedded in a glass matrix. As a result, the experimental μ_r and ε_r of the synthesized ferrite disk were measured to be 2.59 and 5.7, respectively, at 2.5 GHz, as shown in Fig. 16. It is noted that the experimental μ_r is close to the calculated theoretical μ_r, and the experimental ε_r is also in the range of 4.5 to 7.0 for the designed ε_r.

3.3. Performance of RPA

Fabricated ferrite 1-RPA was simulated and characterized for antenna performance. The simulation data, S_{11}, are in good agreement with the experimental data, as shown in Fig. 17, thus indicating the resonant frequency of 2.7 GHz with the mode-3 radiation pattern. Moreover, the simulated and measured gain pattern of 1-RPA at 2.7 GHz, as shown in Fig. 18(a), clearly represent a well-separated gain of the mode-3 radiation pattern. This corresponds to the simulated inner-electric field distribution, which is shown in Fig. 18(b). Consequently, the ferrite 1-RPA volume is reduced to 14.5% of the dielectric UT 2-CPA volume of 95 cm^3 [6].

Furthermore, the ferrite 2-RPA with a 150° angle between ports 1 and 2 was designed as shown in Fig. 1(c) and simulated for antenna performance. Simulation results in Fig. 19(a) indicate that the 2.45 GHz of f_c and -40 dB of isolation are suitable for W-LAN MIMO applications. The measured isolation between port 1 and

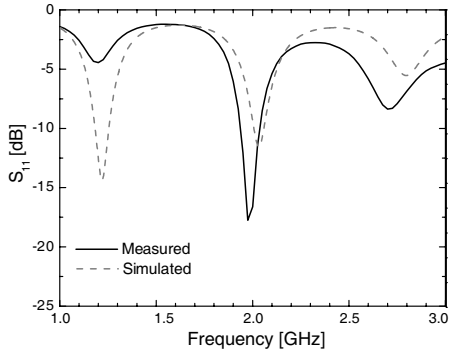

Figure 17. Simulated and experimental S_{11} spectra of ferrite 1-RPA.

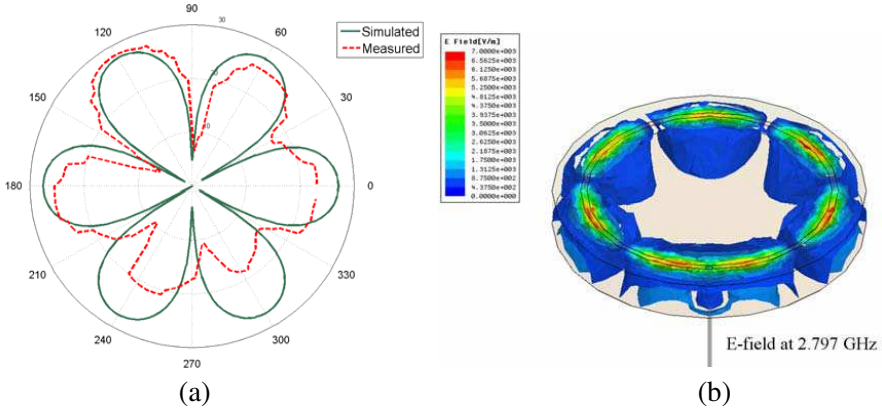

Figure 18. (a) Experimental gain pattern for 1-RPA and (b) simulation result of inner-electric field distribution in 1-RPA.

2 was −37 dB at the mode 3 resonant frequency. Both simulated and measured isolations were similar. Fig. 19(b) shows the weak orthogonal gain pattern simulated in the far-field range. However, Fig. 20 shows six well-distinguished, strong electric field spots for each ring radiator. This confirms mode 3 radiations in the near-field region, even though radiation patterns are mixed in the far-field region. The channel capacity of MIMO system can be reduced by the mixed radiation patterns. However, excellent isolation −40 dB between ports 1 and 2 were obtained due to part of unmixed radiation patterns in 3 dimensional space. It is noted that correlation between radiation patterns from ports 1 and 2 can be minimized by orthogonal radiation in the near-field region as shown in Fig. 21. The correlation coefficient

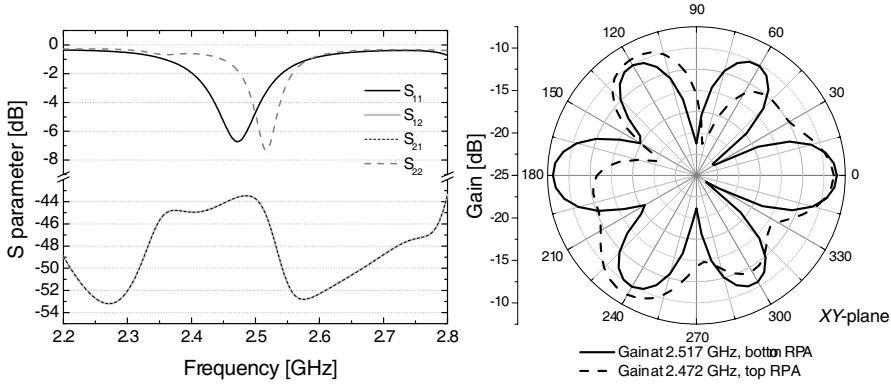

Figure 19. (a) S parameters and (b) gain patterns for ferrite 2-RPA.

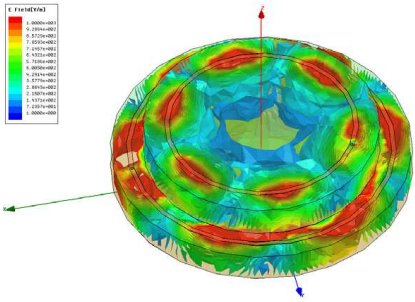

Figure 20. Inner-electric field distribution of 2-RPA at 2.45 GHz.

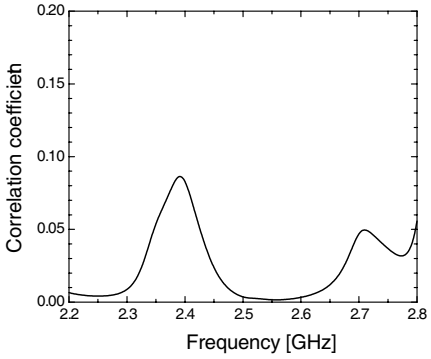

Figure 21. Calculated correlation coefficient of 2-RPA.

(ρ_e) of 2-RPA is calculated by Equation (17), which can be applied to compute the envelope correlation of any two-port antenna diversity system [35], and is 0.036 at 2.5 GHz.

$$\rho_e = \frac{\left|S_{11} * S_{12} + S_{21} * S_{22}\right|^2}{\left(1 - \left(\left|S_{11}\right|^2 + \left|S_{21}\right|^2\right)\right)\left(1 - \left(\left|S_{22}\right|^2 + \left|S_{12}\right|^2\right)\right)} \tag{17}$$

In this calculation, $4.5 \sim 7.0$ of ε_r and $2.2 \sim 2.3$ of μ_r were used for the ferrite 2-RPA, and these values are experimentally achievable.

For comparison, antenna size, resonant frequency, and antenna performance of the dielectric 2-CPA and ferrite 2-RPA are given in

Table 3. Comparisons of calculated antenna performance between UT antenna [6] and proposed antennae.

	Dielectric 2-CPA [6]	Ferrite 2-RPA
Volume [cm^3]	95.0 (100 %)	34.5 (36.3 %)
Area [cm^2]	350.8 (100 %)	32.0 (9.1 %)
Radius of Disk 1 [cm]	5.28	3.19
Height of Disk 1 [cm]	0.9	0.65
μ_r of Disk 1	1 (no loss)	2.2 (loss tanδ = 0.01)
ε_r of Disk 1	2.2 (no loss)	4.5 (loss tanδ = 0.001)
Radius of Disk 2 [cm]	2.70	2.5
Height of Disk 2 [cm]	0.7	0.7
μ_r of Disk 2	1 (no loss)	2.3 (loss tanδ = 0.01)
ε_r of Disk 2	8 (no loss)	7.0 (loss tanδ = 0.001)
f_c [GHz]	2.45	2.5
Bandwidth [MHz] at VSWR 3	180	71
Maximum Gain [dBi], Radiation Efficiency [%]	3.80 dBi, 240%	–1.92, 64.3%
Mode	3	3

Table 3. These results strongly suggest that the use of ferrite material can dramatically reduce antenna volume. The ferrite 2-RPA volume is three times smaller than the dielectric 2-CPA volume.

4. CONCLUSION

Miniaturization of the ferrite 1- and 2-RPAs was successfully accomplished with the Z-type hexaferrite ($Ba_3Co_2Fe_{24}O_{41}$). The antenna volumes were 14.5% and 34.5% smaller than those of the dielectric 2-CPA volume (95.0 cm^3), respectively. Also, mode-3 orthogonal radiation from the ferrite 1-RPA was confirmed. The Z-type barium hexaferrite ($Ba_3Co_2Fe_{24}O_{41}$)-borosilicate glass composite was developed for the RPAs and its permeability and magnetic loss were 2.59 and 0.03, respectively, at 2.5 GHz. Low magnetic loss ferrite is under investigation to achieve high gain for 2-RPA.

The isolation of the ferrite 2-RPA was -40 dB. This excellent isolation property is attributed to the mode-3 radiation of both top and bottom ferrite RPAs with $30^\circ + 60^\circ N$ angle between lobes. Therefore, the miniaturized ferrite 2-RPA with Z-type hexaferrite-borosilicate glass composite can be an antenna solution to MIMO communication systems.

ACKNOWLEDGMENT

This work was supported by NASA EPSCoR under grant NNX08AV84A.

REFERENCES

1. Bhatti, R. A., J. H. Choi, and S. O. Park, "Quad-band MIMO antenna array for portable wireless communications terminals," *IEEE Antennas and Wireless Propagation Letters*, Vol. 8, 129–132, 2009.
2. Chung, K. and J. H. Yoon, "Integrated MIMO antenna with high isolation characteristic," *Electronics Letters*, Vol. 43, No. 4, 199–201, 2007.
3. Vaughan, R. G., "Two-port higher mode circular microstrip antenna," *IEEE Trans. Antennas Prop.*, Vol. 36, 309–321, Mar. 1988.
4. Vaughan, R. G. and J. B. Anderson, "A multiport patch antenna for mobile communications," *Proc. 14th European Microwave Conference*, 607–612, 1984.
5. Forenza, A. and R. W. Heath, Jr., "Benefit of pattern diversity via two-element array of circular patch antennas in indoor clustered MIMO channels," *IEEE Trans. on Comm.*, Vol. 54, 943–954, May 2006.
6. Forenza, A. and R. W. Heath, Jr., "Optimization methodology for designing 2-CPAs exploiting pattern diversity in clustered MIMO channels," *IEEE Trans. on Comm.*, Vol. 56, No. 10, 1748–1759, 2008.
7. Bae, S., Y. K. Hong, and A. Lyle, "Effect of Ni-Zn ferrite on bandwidth and radiation efficiency of embedded antenna for mobile phone," *J. Appl. Phys.*, Vol. 103, 07E929, 2008.
8. Bae, S., Y. K. Hong, J. J. Lee, J. Jalli, G. S. Abo, W. M. Sung, G. H. Kim, S. H. Park, J. S. Kum, and H. M. Kwon, "Co_2Z hexaferrite T-DMB antenna for mobile phone applications," *IEEE Trans. Magn.*, Vol. 45, No. 10, 4199–4203, 2009.
9. Kim, Y., S. Bae, and J. R. Kim, "Effect of ferrite substrate on antenna miniaturization," *J. Korean Phys. Soc.*, Vol. 52, 127–141, 2008.
10. Mahmud, S. T., A. K. M. Akther Hossain, A. K. M. Abdul Hakim, M. Seki, T. Kawai, and H. Tabata, "Influence of microstructure on the complex permeability of spinel type Ni-Zn ferrite," *J. Magn. Magn. Matr.*, Vol. 305, 269–274, 2006.

11. Kulkarni, D. C., S. P. Patil, and V. Puri, "Properties of $Ni_xZn_{(1-x)}Fe_2O_4$ thick films at microwave frequencies," *Microelectronics J.*, Vol. 39, 248–252, 2008.
12. Tsutaoka, T., T. Kasagi, and K. Hatakeyama, "Magnetic field effect on the complex permeability for a Mn-Zn ferrite and its composite materials," *J. Euro. Ceramic Soc.*, Vol. 19, 1531–1535, 1999.
13. Thakur, A., P. Mathur, and M. Singh, "Study of dielectric behavior of Mn-Zn nano ferrites," *J. Phys. and Chem. of Solids*, Vol. 68, 378–381, 2007.
14. Zhao, H., J. Zhou, and L. Li, "Complex permeability spectra of Co-substituted lithium zinc perminvar ferrite," *Key Eng. Mat.*, Vol. 368–372, 591–593, 2008.
15. Ramesh, B. and D. Ravinder, "Electrical properties of Li-Mn ferrites," *Mat. Letters*, Vol. 62, 2043–2046, 2008.
16. Bush, G. G., "The complex permeability of a high purity yttrium iron garnet sputtered thin film," *J. Appl. Phys.*, Vol. 73, 6310–6311, 1993.
17. Krupka, J., S. A. Gabelich, K. Derzakowski, and B. M. Pierce, "Comparison of split post dielectric resonator and ferrite disc resonator techniques for microwave permittivity measurements of polycrystalline yttrium iron garnet," *Meas. Sci. Technol.*, Vol. 10, 1004–1008, 1999.
18. Kim, C. W. and J. G. Koh, "A study of synthesis of NiCuZn ferrite sintering in low temperature by metal nitrates and its electromagnetic property," *J. Magn. Magn. Matr.*, Vol. 257, 355–368, 2003.
19. Wang, H., J. Liu, W. Li, J. Wang, L. Wang, L. Song, S. Yuan, and F. Li, "Structural, dynamic magnetic and dielectric properties of $Ni_{0.15}Cu_{0.2}Zn_{0.65}Fe_2O_4$ ferrite produced by NaOH co-precipitation method," *J. Alloys and Compounds*, Vol. 461, 373–377, 2008.
20. Shepherd, P., K. K. Mallick, and R. J. Green, "Magnetic and structural properties of M-type barium hexaferrite prepared by co-precipitation," *J. Magn. Magn. Matr.*, Vol. 311, 683–692, 2007.
21. Mallick, K. K., P. Shepherd, and R. J. Green, "Dielectric properties of M-type barium hexaferrite prepared by co-precipitation," *J. of Euro. Ceramic Soc.*, Vol. 27, 2045–2052, 2007.
22. Bae, S., Y. K. Hong, J. J. Lee, J. Jalli, G. S. Abo, A. Lyle, W. M. Seong, and J. S. Kum, "Low loss Z-type barium ferrite (Co_2Z) for T-DMB antenna application," *J. Appl. Phys.*, Vol. 105, 07A515, 2009.

23. Bae, S., Y. K. Hong, J. J. Lee, J. Jalli, G. S. Abo, A. Lyle, I. T. Nam, W. M. Seong, J. S. Kum, and S. H. Park, "New synthetic route of Z-type ($Ba_3Co_2Fe_{24}O_{41}$) hexaferrite particles," *IEEE Trans. Magn.*, Vol. 45, No. 6, 2557–2560, 2009.
24. Bai, Y., J. Zhou, Z. Gui, and L. Li, "Magnetic properties of Cu, Zn-modified Co_2Y hexaferrites," *J. Magn. Magn. Matr.*, Vol. 246, 140–144, 2002.
25. Bai, Y., J. Zhou, Z. Gui, L. Li, and L. Qiao, "The physics properties of Bi-Zn codoped Y-type hexagonal ferrite," *J. Alloys and Compounds*, Vol. 450, 412–416, 2008.
26. Lin, C.-S., C.-C. Hwang, T.-H. Huang, G.-P. Wang, and C.-H. Peng, "Fine powders of $SrFe_{12}O_{19}$ with $SrTiO_3$ additive prepared via a quasi-dry combustion synthesis route," *Mat. Sci. and Eng. B*, Vol. 139, 24–36, 2007.
27. Balanis, C. A., *Antenna Theory: Analysis and Design*, 2nd edition, Wiley, New York, 1982.
28. Ikonen, P. M. T., K. N. Rozanov, A. V. Osipov, P. Alitalo, and S. A. Tretyakov, "Magnetodielectric substrates in antenna miniaturization: Potential and limitations," *IEEE Trans. on Ant. and Prop.*, Vol. 54, 3391–3399, Nov. 2006.
29. Hansen, R. C. and M. Burke, "Antenna with magneto-dielectrics," *Microwave Opt. Technol. Lett.*, Vol. 26, No. 2, 75–78, 2000.
30. Chu, L. J., "Physical limitations of omni-directional antennas," *J. Appl. Phys.*, Vol. 19, 1163–1175, 1948.
31. Mclean, J. S., "A re-examination of the fundamental limits on the radiation Q of electrically small antennas," *IEEE Trans. on Ant. and Prop.*, Vol. 44, 672–675, May 1996.
32. Ziolkowski, R. W. and A. Erentok, "At and below the Chu limit: Passive and active broad bandwidth metamaterial-based electrically small antennas," *IET Microw., Ant. and Prop.*, Vol. 1, 116–128, Feb. 2007.
33. Caimi, F. M., "Theoretical size constraints for antennas based on quality factor Q," Released document by IEEE P802.15 working group, IEEE 802.15 < 02/295 >, July 2002.
34. Walser, R. M., W. Win, and P. M. Valanju, "Shape-optimized ferromagnetic particles with maximum theoretical microwave susceptibility," *IEEE Trans. Magn.*, Vol. 34, 1390–1392, 1998.
35. Blanch, S., J. Romeu, and I. Corbella, "Exact representation of antenna system diversity performance from input parameter description," *Electron Lett.* Vol. 39, 705, 2003.